Tritiated thymidine internalization in zebrafish early life stages: joint use of experimental procedures and microdosimetry

M. Schiano Di Lombo, Isabelle Cavalie, Virginie Camilleri, Y. Perrot, Beatrice Gagnaire

Title: Tritiated thymidine internalization in zebrafish early life stages: joint use of experimental procedures and microdosimetry

Running title: Tritiated thymidine internalization in zebrafish

Schiano Di Lombo Magali[1], Cavalie Isabelle[1], Camilleri Virginie[1], Perrot Yann[2], Gagnaire Beatrice[1]

Affiliations

[1] Institut de Radioprotection et de Sûreté Nucléaire (IRSN), PSE-ENV/SRTE/LECO, Cadarache, 13115, Saint-Paul-lez-Durance, France

[2] Institut de Radioprotection et de Sûreté Nucléaire (IRSN), PSE-SANTE/SDOS/LDRI, 92262 Fontenay-aux-Roses CEDEX, France

***Corresponding author: Schiano Di Lombo Magali** (magali.schianodilombo@gmail.com)

Keywords: Tritium, zebrafish, microdosimetry, organically bound tritium, internalization, DNA, tritiated thymidine

Abstract

Schiano Di Lombo M., Cavalie I., Camilleri V., Perrot Y. and Gagnaire B. Tritiated thymidine internalization in zebrafish embryo and larva: joint use of experimental processes and microdosimetry. *Radiat. Res.*

Tritium is found in the environment under three forms: free in the water, gaseous, and bound to organic matter. Once internalized in living organisms, it can be found in two forms: Tissue Free Water Tritium (TFWT) and Organically Bound Tritium (OBT). This study aims to better understand OBT internalization in living organisms and to show the complementarity between experimental procedures and microdosimetry simulations that have often been used in order to obtain more information on imparted energy to cell nuclei. To do so, tritiated thymidine, an organic form of tritium, was chosen and zebrafish embryos (3.5 hpf; hours post fertilization) were exposed to a range of activity concentrations ($2.21x10^3$ to $5.95x10^5$ Bq/mL). First, individuals were sampled after different exposure times (1 to 96 hours of exposure) in order to qualify the internalization kinetics. Then, the barrier role of the chorion was assessed after 2 days of exposure. Lastly, individuals were sampled after 1 and 4 days of exposure in order to measure the internalization in the whole fish and its DNA, but also to highlight a possible link between the internal dose rate and the external activity concentration. Microdosimetry simulations were also made in order to quantify the imparted energy that could occur in the zebrafish cells after exposure to tritium. Results showed that when bound to thymidine, tritium rapidly incorporates in zebrafish early life stages, with the internalization being almost complete after 24 hours. Results also showed that while the chorion acted as a barrier to prevent thymidine from entering the embryos, significant levels could still be measured in the whole organisms as well as in DNA. This study also highlighted that when the external activity concentration

increased, the internal dose rate increased as well, following a sigmoidal trend. Microdosimetry simulations highlighted that the size and shape of the cell matters, and that the smallest cells seem to be at the greater risk, with only low-energy electrons inducing energy depositions. A linear fit was also found between the mean energy deposited and the logarithm of the radius of the cell, thus showing that the quantity of deposited energy is proportional to the radius of the cell. While this study highlighted important internalization pattern, it will also be used as the starting point of a study focusing on the toxic effects of tritiated thymidine on zebrafish in its early life stages.

1. Introduction

Tritium is the only hydrogen isotope with radioactive properties (1). It is a β-emitter that has a half-life of 12.3 years, and a mean energy of 5.7 keV. Considering that it is a hydrogen isotope, its physico-chemical properties are the same than that of hydrogen, meaning it could be found in every environmental compartments (2). In the environment, tritium can be found in three main forms: free in the water (HTO), gaseous tritium (HT) and organically bound tritium (OBT), where tritium replaces hydrogen in an organic molecule. Tritium is produced by natural and anthropogenic processes. In the environment, its main anthropogenic sources are nuclear industries such as nuclear power plants, which routinely release tritium as HTO (3–5). Tritium levels in all the environmental compartments have been monitored in France for many years, highlighting basal levels of 0.12 to 0.86 Bq/L (6,7). Under a radioactive influence, tritium levels were of 1 to 61 and 5 to 35 Bq/L in the Rhône and Garonne rivers, respectively .When the tritium enters the biological tissues, it can be found in three different forms: Tissue Free Water Tritium (TFWT), where tritium is trapped in the tissue water; exchangeable-organic tritium (eOBT), where a tritium is bound to oxygen, sulfur, nitrogen or phosphorous; and non-exchangeable organic tritium (neOBT), where tritium is bound to a carbon atom (8). The latter is the tritium form that has the highest biological half-life.

Considering that tritium can enter living organisms, many studies have focused on internalization measurements, both on the field and in the laboratory (3,5,8–12). A study focusing on the HTO internalization in zebrafish embryos and larvae have shown that tritium does incorporate in the tissue of the animals at a fast rate, and is mainly found in the form of TFWT (3). It was also shown that when living organisms are exposed to both HTO and OBT, high tritium levels were found in mussel and fish ((9.92 - 22.9)x10^4 Bq/kg and (2.10 - 24.00)x10^4 Bq/kg, respectively) (9). Multiple studies have also focused on the

internalization differences between HTO and OBT, highlighting the fact that OBT contributes more to the absorbed tritium dose compared to HTO (8,10–12). Those studies also showed that both compounds behave differently, with TFWT reaching equilibrium with the external activity concentration while OBT does not, leading to longer depuration rates measured in the latter case.

Tritiated organic compounds as tritiated thymidine have been used in order to better understand biological mechanisms. As thymidine is a thymine precursor, DNA internalization is expected, leading to its use in studies focusing on DNA synthesis (13–19). Many of those studies have shown that as expected, significant tritium levels could be measured in the cell and in the DNA after an *in vitro* exposure of those cells to the labelled nucleoside. Two of those studies also highlighted the fact that thymidine enters the cell via the salvage pathway, also known as facilitated diffusion (15,17). When thymidine reaches the cell, two competing mechanisms occur. Either the thymidine is directly transformed into thymine, leading to its degradation before it can be internalized into the DNA, or it is rapidly phosphorylated and joins the derivative pool, which is the intermediate between the thymidine internalization in the cell and its internalization in the DNA (15,16,19). While a major part of the thymidine is directly transformed into thymine before being taken out of the cell, thymidine phosphorylation is still significant, as it enables the DNA synthesis. But while the thymidine phosphorylation is fast, it is still dependent on the thymidine transport system that is itself dependent on the cell cycle. Indeed, it seems that the tritiated thymidine internalization in the cell is almost null in the G1-phase, before strongly increasing when the cells reach the S-phase and decreasing when the cells enter the G2-phase (14–16,18). As explained above, these studies concluded that tritium linked to thymidine can enter the cell and the DNA.

Quantification tools as liquid scintillation can be used in order to obtain more information on radioactive levels in different organisms. But, in order to understand all the damages that can occur after an exposure to radiation, this information is not sufficient. Biological effects and internalization should be linked to an actual value of energy deposited. When considering that the sensitive volume is the cell, the energy deposit by decay will have a marked stochastic nature. Microdosimetric formalism is then relevant in order to obtain information on the imparted energy distribution at the microscopic level (20). Indeed, microdosimetry gives the formalism necessary to describe the distribution of the energy depositions that occur stochastically in a given target, and it can be used to analyse the imparted energy at the cell scale (21,22). Such cellular simulations are even more important when considering beta-emitters as tritium (4,20,23–25). Indeed, a study has proven that microdosimetric simulations can highlight important differences in energy depositions in materials as Teflon® or water (25). This study showed that the range of beta-rays emitted from tritium were 35 times shorter than the one emitted from Carbon-14, with the total energy released by tritium being absorbed in spherical volumes of Teflon or water way smaller than in the case of Carbon-14. As beta-rays emitted by tritium cannot travel high distances (*i.e.* around 7 µm in soft tissues for the most energetic rays), the calculated absorbed doses in the decay vicinity of H-3 were found to be very high, thus showing that microdosimetric considerations are important for the evaluation of the radiolytic effectiveness of beta-emitters as tritium (23,25). Other studies also highlighted differences between HTO and OBT by the means of microdosimetry (4,23,24). Significative differences were found between HTO and OBT, specifically when the target size gets smaller, partly because OBT is heterogeneously distributed in the organism, leading to more complex microdosimetric cases.

The main objective of this study was to quantify tritiated thymidine internalization in zebrafish in its early life stages. With this purpose, the tritiated thymidine internalization in the organisms was studied by means of experimental procedures and microdosimetric simulations. The use of both approaches was also chosen in order to answer another objective: showing how experimental processes and simulations could complete each other. Zebrafish was chosen as it is a convenient laboratory species, with adults being able to spawn hundreds of eggs in a single spawning, and the genome of this species being fully sequenced (26,27). Early developmental stages were chosen as they are considered as being more sensitive to a large range of chemicals. Also, the first developmental stages have already been studied, giving u the required information for the microdosimetric simulations (28,29). In order to study the tritium internalization in the zebrafish embryos and larvae, zebrafish embryos were exposed to a large range of tritiated thymidine activity concentrations ($2.21x10^3$ to $5.95x10^5$ Bq/mL). During those exposures, individuals were sampled after different exposure times in order to have more information on the internalization kinetics. Moreover, individuals were sampled after 1 and 4 days of exposure in order to quantify the tritium internalization in the whole individual, but also in its DNA, which was quantify after extraction. Finally, microdosimetric simulations were made in order to obtain more information on the imparted energy at a cellular level, giving more information on which cells could be more at risk when chronically exposed to tritiated thymidine.

2. Material and methods

2.1. Fish

All experimental procedures performed in this study were previously approved by IRSN Animal Care Committee and followed French regulations for animal

experimentation (protocol P2019-19; registration number of IRSN laboratory: C13-013-07). Four months old wild-type zebrafish (AB genetic background) were supplied by Paris Sorbonne University (France) and were kept in a zebrafish housing system (Zebtec Techniplast® Stand Alone) with a 12:12h light:dark cycle photoperiod. The fishes were fed three times a day with Gemma Wean 0.3 (Skretting). Water parameters were monitored daily (pH 7.5 ± 0.2; conductivity 400 ± 20 µS.cm^{-1}, temperature 27.5 ± 0.2 °C). As males and females were kept in different tanks, the mating was done every three to four weeks to ensure that the fishes had a good reproductive capacity and that the females stayed in good health. All matings were done in the husbandry using the water from the housing system and using fishes that were between 4 and 13 months old.

2.2. Embryo exposure and tritium contamination

Exposures to different tritium activities were done separately to ensure that there was no cross-contamination between the different glass crystallisers. Embryo medium was prepared using InstantOcean sea salt at a concentration of 60 mg/L (30). The embryo medium was used as the negative control condition and to dilute the tritiated thymidine source. Tritiated thymidine solution (97% purity, 185 MBq, PerkinElmer, Courtaboeuf, France) was diluted in embryo medium to obtain final activity concentrations varying between 2.21 x 10^3 and 5.94 x 10^5 Bq/mL.

The exposure was designed from the protocol described in Arcanjo et al (3). At 3.5 hpf, zebrafish eggs were placed in two glass crystallisers covered with Parafilm at a density of two eggs per mL of tritiated thymidine solution or embryo medium. The eggs were kept in the dark in thermo-regulated incubators (Heraterm, ThermoScientific) at 27 ± 1 °C for 4 days. At 48 h, 80 % of the water medium was renewed with fresh solutions. Tritium-free water (Abatilles water, France) was also placed in the incubators (40 mL/beaker) in order

to monitor tritium exchanges in the incubator. Temperature (°C) and relative humidity (%) were monitored every 30 minutes during the exposure (HOBO data logger U12, Onset).

Tritium measurements were made on the medium (3 replicates/crystalliser, once a day, 10 µL of medium in 990 µL of tritium free water), on the tritium-free water (1 replicate/beaker, once a day, 1 mL) and on the eggs and larvae (24 and 96 hpe, hours post exposure). Blank measurements were made on tritium-free water (Abatilles water, France). After adding 19 mL of the liquid scintillation cocktail (Ultima Gold LLT, Perkin Elmer), the liquid scintillation measurements were done using a Quantulus (Quantulus 1220, Perkin Elmer) monitored by WinQ (1220-307 WinQ, Perkin Elmer). Each measurement was done three times and lasted 20 minutes. The data were processed using the EasyView software. The results were expressed as Bq/mL.

2.3. Internalization measurements

2.3.1. Tritium internalization kinetics and barrier function of the chorion

Tritium kinetics measurements were realised on 10 to 15 individuals that were exposed during 1 to 96 hours (1; 3; 6; 20; 22; 24; 48; 72 and 96 h) to tritiated thymidine at a concentration activity of $(4.2 \pm 0.3)x10^4$ Bq/mL. For the negative control, only 3 individuals were sampled at each time point. The internalization was measured according to a protocol modified from the one described by Arcanjo et al. (3). Briefly, 10 to 15 individuals were sampled and individually dried on a filter (RA 1.2, Millipore). With a needle, the egg was rolled over the filter while the larva was only gently taped on the filter. Once the sample was dry, it was placed in a liquid scintillation tube. One mL of soluene-350 (Perkin Elmer) was added to the sample that was then left to heat for 48 hours at 55 °C. In a next step, 35 µL of glacial acetic acid (Sigma Aldrich) was added, followed by 19

mL of Ultima Gold LLT scintillation liquid (Perkin Elmer). All results were expressed as Bq/sample.

After 48 hours of exposure to solution with tritium activity concentrations of $3.4x10^3$ and $4x10^4$ Bq/mL, two types of samples were dried and mineralized. Firstly, 15 whole embryos were dried as explained above. Secondly, 15 other individuals were sampled and the chorion was carefully removed before sampling the larvae and drying it by taping it on a filter. All samples were mineralized following the process explained above. Results were processed using the EasyView software and were expressed as Bq/sample.

2.3.2. Tritium internalization measurements: 24 and 96 hours of exposure

The internalization measurements were realised on 20 to 30 individuals that were exposed during 24 hours (24 hpe) to tritiated thymidine at concentration activities ranging from $2x10^3$ to $6.5x10^5$ Bq/mL (0.2; 3.3; 4.9; 6.5; 6.6; 9; 11; 15; 33 and $65x10^4$ Bq/mL). For the negative control, only 6 individuals were sampled at each time point. The internalization was measured according to a protocol modified from the one Arcanjo et al. (3). Briefly, 30 embryos were sampled and individually dried on a filter (RA 1.2, Millipore) as explained above. Briefly, 10 to 15 tubes were used for total tritium measurement and another 10 to 15 were used to measure OBT. For total tritium measurement, samples were processed as described above and for the OBT measurements, samples were firstly dried in opened tube for 48 h at 55 °C before following the same protocol described for total tritium quantification. All samples were measured using a Quantulus monitored by WinQ. The results were processed using the EasyView software. For the larvae exposed for 96 hours to the same activity concentrations, only 10 to 15 samples were dried and only the total tritium internalization was measured.

Results were expressed in Bq/kg (fresh weight) using weight data presented by Arcanjo et al. (3). Dose rate (DR, µGy/h) were calculated using the equation:

$$DR = (DCC_{ext} \times A_w) + (DCC_{int} \times A_O) \qquad (1)$$

where A_w is the tritium content in the water (Bq/mL), DCC_{ext} is the calculated dose coefficient related to external exposure (µGy/h per Bq/g), A_O is the tritium content in the organism (Bq/g, fresh weight) and DCC_{int} is the calculated dose coefficient related to internal exposure (µGy/h per Bq/g). The dose coefficients (DCs) were calculated by analytical procedure using EDEN v3 (developed by IRSN (31)), following the hypothesis that tritium is homogeneously distributed in the organism. These DCs and weights used are presented in Table 1. Concentrations factors (CF, mL/g) were calculated following this equation:

$$CF = \frac{A_O}{A_w} \qquad (2)$$

Where A_O is the tritium content in the organism (Bq/g, fresh weight) and A_w is the tritium content in the water (Bq/mL).

2.3.3. DNA extraction and tritium measurements

DNA was extracted from zebrafish embryos and larvae following the DNeasy® Blood & Tissue Kit (Kiagen). Briefly, 3 pools of 25 control embryos (or 18 larvae) and 5 pools of 25 contaminated embryos (or 18 larvae) were sampled after being rinsed with clean embryo medium that was then removed and replaced by 200 µL of a Buffer ATL/Proteine K mix (90:10, v/v). 200 µL of Buffer AL were added, followed by 200 µL of Ethanol (> 96 %). The mixture was then added to a DNeasy Mini spin column placed in a 2 mL collection tube. The sample was centrifuged for 1 min at 6000 g at room temperature. The supernatant was then discarded and then spin column was placed in a new 2 mL collection tube before adding 500 µL of Buffer AW1 and centrifuging the sample at 6000 g for 1 min.

The supernatant was discarded, and the spin column was added to a new 2 mL collection tube. Buffer AW2 (500 µL) was added in the column and the sample was centrifuged for 3 min at 20000 g. The column was placed in a 2 mL microcentrifuge tube and the DNA was eluted by adding 50 µL of Buffer AE to the center of the spin column membrane. The DNA was left to incubate at room temperature for 1 minute before being centrifuged for 1 min at 6000 g.

DNA concentration (µg/mL) was measured using the Qubit® dsDNA Broad Range Assay Kit (ThermoFisher Scientific). All samples are treated individually, and two DNA standards (0 and 100 ng/µL in TE buffer) were added. In each 0.5 mL tube, 190 µL of the dsDNA BR Reagent/dsDNA BR Buffer mix (1:199, v/v) were mixed with 10 µL of the DNA sample. Each sample was vortexed before being incubated in the dark at room temperature for 5 minutes. The Qubit® 3.0 Fluorometer was used to measure the DNA concentration in the sample. Extracted DNA (25-35 µL) was mixed with Abatilles water (965-975 µL) and the tritium activity concentration was measured following the protocol already presented for the tritium liquid measurements.

2.4. Microdosimetry simulations

In the formalism used in this study, the energy released to a volume is the imparted energy noted Ɛ. It is the sum of all the elementary energy deposits in this volume coming from a primary particle (in our case an electron from the decay) and from all the secondary particles. For each cell, Ɛ is a stochastic variable, also leading to different specific energies (z) which is the microdosimetric quantity equivalent to the absorbed dose. It is worth pointing out that absorbed dose D corresponds to the ratio between the mean value of the deposited energy in the matter and the mass of the volume where the deposition occurs.

In this work, simulations were computed using Geant4 Monte Carlo toolkit version 10.06 as well as its extension, Geant4-DNA. This extension proposes, among other things, physical models at very low energy for the simulation of the track structure (i.e. the spatial distribution of the interactions points) in liquid water and which is thus well adapted to microdosimetry (32–37). Geant4 Monte Carlo toolkit has been chosen as both ellipsoidal and spherical cells are usable, which is not the case with MIRDcell, but different studies showed that Geant4 can be used instead of MIRDcell as the results obtained are comparable (37,38). For microdosimetric calculation the shape and size of the target volume have a strong impact on the distribution of the imparted energy. In order to simulate the cells present in the zebrafish embryos and larvae, an individual cell was represented as a sphere or an ellipsoid made of liquid water, considering the majority of zebrafish cells are of those shapes. The radius chosen were from 0.25 to 10 µm (0.25; 0.5; 1.25; 2.5; 5; 7.5; 10 µm) for the spherical cells and from 0.5 to 15 µm (0.5; 2.5; 5; 7.5; 10; 12.5; 15 µm) for the ellipsoidal ones (22,39–54). The radius chosen for the ellipsoidal cells corresponds to the smallest of the three axes, the other characteristic dimensions being taken equal to twice this radius (x = radius; y = 2xradius; z = 2xradius). Simulations were made in liquid water on one cell of interest made of liquid water while considering the presence of its neighbour cells, with the cell of interest being in the middle of a 3-D cell cluster. The presence of the neighbour cells was taken into consideration as a study made on the tritiated thymidine incorporation in rhesus monkeys *(Macaca mulatta)* showed that labelled cells are usually close to each other, forming bands (13). For those neighbour cells, it was taken into account that electrons released by tritium during its decay can only travel up to 6 µm in liquid water (55) and the cells located at a distance greater than 6 µm were therefore not taken into account. For those simulations, 10^6 electrons were being released in the cell of interest but also in its neighbours. The simulation scheme is represented in Figure 1. As a large number

of electrons were used in the simulations, the simulation is quite robust, and its statistic error is 1.5 %.

From these simulations, the probability of having an imparted energy for one tritium disintegration from 50 to 18500 eV (with a 50 eV bin) was obtained. This energy scale was chosen considering that electrons emitted by tritium during its decay have a maximum energy of 18.6 keV (55). These simulations also indicated the mean imparted energy in each cell, the imparted energy having the highest probability and the maximum energy that could be deposited in the cell. In this work, the mean imparted energy will be expressed in eV per disintegration and represented as a function of the radius of the cell.

2.5. Statistical analyses

Statistical analyses were performed using RStudio with PMCMR, car and lmtest packages. All data were expressed as mean ± SD (Standard Deviation). Packages as ggplot2, ggpubr, ggmisc and scales were used to represent the data as graphs. The normality of data distribution and the homogeneity of the variances were verified using the Shapiro-Wilks and Levene tests ($p < 0.05$). For the water tritium content during the experiment, a two-way ANOVA was performed with crystallizer and time as factors. When necessary, this test was followed by a Tukey post-hoc test ($p < 0.05$). To compare the total tritium and OBT contents in the zebrafish embryos and larvae, t-test or Wilcoxon test were performed ($p < 0.05$). Lastly, to compare the concentration factors between each experiment, a one-way ANOVA was performed, followed by a Nemenyi post-hoc ($p < 0.05$) when necessary. To compare the tritium concentrations measured in the DNA between the different tritium activity concentrations, the Kruskal-Wallis test was performed, followed by a Bonferroni post-hoc test ($p < 0.05$).

3. Results

3.1. Tritium internalization in zebrafish early stages

3.1.1. Tritium internalization kinetics and barrier function of the chorion

Tritium internalization kinetics measured after the first experiment are presented in Fig. 2A. These results gave the general trend, showing that there was a first significant increase in the internalization between 0 and 1 hour of exposure. The internalization then reached a threshold between 1 and around 6 hours of exposure. It then increased again between 6 and 24 hours of exposure before slowing down before 48 hours of exposure. Considering the large standard deviations measured at 22, 24 and 48 hours, the experiment was repeated using a similar activity concentration ($4.0x10^4$ instead of $4.5x10^4$ Bq/mL) and more individuals (15 instead of 10) were sampled. The results are exposed in Fig. 2B. These results confirmed the trend already observed after the first experiment, and tritium activity concentrations in the sample statistically different between samples exposed for 1 and 24 hours ($p < 0.001$).

In order to verify the hypothesis of the chorion acting as a barrier, the activity was measured by removing the chorion of half of the individuals after 48 hours of exposure, before mineralization. For both external activities tested, the activity measured in the individual without the chorion was significantly lower than the activity measured in the individual with the chorion (2.03 vs 44.71 and 11.09 vs 171.17 Bq for $3.3x10^3$ and $4x10^4$ Bq/mL, respectively; $p < 0.001$).

3.1.2. Tritium internalization in embryos and larvae

Activity concentrations measured in the crystallizers at the beginning of the experiment, measured external activity concentrations and calculated internal dose rates after 24 and 96 hours of exposure are presented in Table 2. Some data are missing either

because they were not planned to be measured, or because there was a technical issue during the experiment. The results showed that for embryos and larvae, the internal dose rate increased with the external activity, but this increase did to seem to be linear. Also, it can be pointed out that the standard deviations for this parameter were higher for embryos compared to larvae. Considering that the increase of the dose rate with the external activity concentration did not seem to be linear, the dose internal dose rate was plotted against the external activity concentration, and those plots are presented in Fig. 4 and Fig. 5. For embryos (Fig. 4) as for larvae (Fig. 5), the tritium internalization seemed to follow a sigmoidal curve, with an exponential increase leading to a saturation point at an external activity concentration of around 2 to $2.5x10^5$ Bq/mL.

The form of the incorporated tritium was also studied by measuring the total tritium and OBT fractions, separately. The results are presented in Table 3. As showed in the table, there were no statistical differences between the total tritium and OBT dose rates ($p > 0.05$).

3.1.3. Tritium internalization in DNA

Tritium incorporation in the DNA from embryos and larva exposed to three tritium activities was measured and the results are presented in Table 4. Tritium incorporation in the DNA was visible even at the lowest external activity concentration measured ($3.46x10^3$ Bq/mL). The results also showed that as for the tritium incorporation in the whole embryo and larvae, the internalization process seemed to be complete after 24 hours of exposure, as there was no significant differences between the tritium activity concentrations in the DNA at 24 and 96 hours of exposure ($p > 0.05$).

3.2. Microdosimetry of tritium in zebrafish cells

For all cells, the highest probability was reached for the lowest imparted energy per disintegration (0-50 eV), and this was observed for all cells, with no effect of their shape or their size (Fig. 6). For all cells, the probability rapidly decreased while the energy increased, until the imparted energy reached 250 eV.Bq^{-1}. At this point, the probability increased, reaching a maximum for imparted energies of 250 and 350 eV.Bq^{-1} in ellipsoidal and spherical cells, respectively. After this point, the probability decreased exponentially while the imparted energy increased. For both cell shapes, the increase of the cell radius was linked to a decrease in the probability linked to the smallest deposited energies. Cells with the lowest radius also reached a null probability for lower energies than cells with higher radii.

For both cell shapes, the specific energy per Bq computed with Geant4-DNA could be linked to the cell radius ($R^2 \geq 0.99$; Fig. 7). The equations computed for the spherical and ellipsoidal cells can be found in the equations (3) and (4), respectively. z is the mean imparted energy and r is the cell radius. For an equivalent radius, the specific energy for 1 Bq of tritium in a spherical cell was lower than the specific energy in an ellipsoidal cell. For both cell shapes, the specific energy decreased when the cell radius increased.

$$z = 0.0956x^{-2.607} \quad (3)$$

$$z = 0.2766x^{3} \quad (4)$$

4. Discussion

4.1. Tritium internalization kinetics

The results highlighted that there are three steps in the internalization kinetics of tritiated thymidine in embryos and larvae. Briefly, the results showed a first internalization

between 0 and 1 hour of exposure, and a second significant internalization between 6 and 24 hours of exposure. The internalization can then be considered as complete as there were no statistical differences between the activity concentration after 24 and 48 hours. These results are in accordance with another study made on HTO, where tritium internalization kinetics showed that a steady-state appeared between 1 and 24 hours of contamination (3). These results are even more interesting considering that the embryos were exposed from the same time (3 to 3.5 hours post fertilization), showing that despite differences in behaviour between OBT and HTO, internalization kinetics stay the same (8,12).

The last part of the kinetic was the significant decrease between 48 and 72 hours of exposure. This could be explained by the hatching that occurred between 48 and 72 hpf, transforming embryos into larvae. We hypothesised that the main fraction of tritium was adsorbed on the chorion, and not internalized in the embryo, which would show a barrier effect of the chorion. This hypothesis was confirmed by the second part of the experiment, with tritium levels being significantly higher in embryos with chorion compared to dechorionated embryos. This result was in accordance with previous studies. The zebrafish chorion has a 3.5 µm thickness and is divided between 3 different layers of different compositions (56). It also contains pores that have a size of 0.17 µm², and its structure is consistent with the roles that have been assigned to its different compartments: diffusive exchange of gases and physical protection, flexible filter for transport of materials and protection against microorganisms (27,57). Considering its composition, its possible barrier function in case of external exposure to pollutants has been investigated, and multiple studies demonstrated that intake of pollutants as polystyrene nanoparticles, lindane or depleted uranium was limited by the chorion (27,58,59).

4.2. Tritium internalization in whole zebrafish embryos and larvae

While studying the tritium internalization, measurements after 24 hours of exposure also showed that tritium is nearly totally internalised in its organic form, which is not surprising considering that tritiated thymidine is an organically bound tritium form. In general, the fact that tritium seemed to be mainly internalised in its organic form strictly differs from HTO studies performed on fish species as rainbow trout (*Oncorhynchus mykiss*) and zebrafish (3,12). Indeed, in the rainbow trout study, Kim et al. showed that significant OBT levels were only obtained after feeding the trout with OBT-spiked food, while a simple HTO exposure in the medium led to high total tritium levels, but no OBT. Arcanjo et al. also showed that the OBT levels were lower after 24 hours of exposure compared to 96 hours of exposure, and that at both times, OBT levels were significantly lower than total tritium ones (3). Those results confirm the main hypothesis of differences in the internalization of OBT and HTO in zebrafish embryos and larvae. These findings are in accordance with a study focusing on tritiated glycine internalization in the mussel (8). It showed that the internalization pattern was different from the one observed in the case of HTO, with a repartition between the different body compartments being different between tritiated glycine and HTO. A few studies focusing on the internalization of OBT through the food chains in different species of fish are also in accordance with our results (9–11). Indeed, those studies, performed on the field and in the laboratory, showed that OBT activity concentrations measured in the fish were higher after the fishes were fed tritiated feed, and that the exposure to HTO did not lead to the measurement of significant OBT levels compared to TFWT. All those studies also confirmed that the depuration rates were lower for OBT compared to HTO.

4.3. Relationship between the internal dose rate and the external activity concentration

Our study showed that the internal dose rate increased exponentially with the external activity concentration before reaching a saturation point. Such results are not surprising, considering those findings had already been made by different studies based on the tritiated thymidine incorporation in different cells. For example, a study focusing on tritiated thymidine internalization in hyperploid Ehrlich ascites tumor cells showed that in the process of incorporating thymidine in the DNA, a precursor pool is formed (19). One study focusing on the same tumor cells found that there was an exponential increase in the tritium internalization when the pool activity concentration increases (16,60). Literature also reported the existence of a saturation point. A study showed that when the thymidine concentration increased in the external medium, the DNA internalized fraction decreased exponentially, thus showing that even at large concentration of thymidine, the internalization will saturate. This is in accordance with the assumption that DNA synthesis depends on a balanced supply of 4 nucleotides, and that the excess of one of those same nucleotides should not cause unbalanced synthesis. Those findings were then confirmed by two other studies, one of them specifying that the excess thymidine might be released out of the cell by a feedback mechanism (15,60). A special care has to be put in such comparisons, as the studies presented above were made using synchronous cell suspensions, which is different from a living organism during its development, where cells are being created at a fast rate (29). It is also important to take into account that the internalization measured in these studies was the direct DNA internalization, while our study mainly focused on the internalization in the whole fish.

4.4. Tritium internalization in the zebrafish DNA

Our study highlighted the fact that even after an exposure to the lowest tritium activity concentration, a significant tritium incorporation could be measured in the DNA. This is in

accordance with a study focusing on the incorporation of tritiated glycine in the marine mussel. It showed that after an exposure to an activity concentration close to our lowest activity concentration, the tritium activity concentration measured in the DNA was similar to the ones we measured in our embryos and larvae (0.05 to 0.2 Bq/µg vs 0.16 to 0.25 Bq/µg, respectively) (8).

Multiple *in vitro* studies have focused on the DNA synthesis rate by using tritiated thymidine incorporation as a synthesis marker (15–17,19,60). In the present study, tritium incorporation in DNA was completed after 24 hours of exposure. Other studies confirmed a rapid incorporation of tritium in DNA (less than one hour) (19,60). A study also highlighted the fact that after one hour of incubation, the radioactivity present in the medium was no longer available for the cell, which could explain the fact that even after the renewal of the medium after 48 hours, no more incorporation was induced (19).

The literature also enabled us to obtain more information on the potential mechanisms leading to the tritiated thymidine incorporation into the zebrafish DNA. Most studies mention the formation of a phosphorylated thymidine pool (16,19,60). This formation is an intermediate step towards the DNA incorporation. A study showed that the pool size is dependent on the tritium external activity concentration, and that an equilibrium is formed between this pool and the external medium in terms of activity concentration (60). Another study also highlighted that while the thymidine is transformed into phosphorylated derivatives before being incorporated into the DNA, there is a competing mechanism in which thymidine is directly transformed into thymine, the latter then being degraded and pushed out of the cell (19). Thymidine is usually mainly transformed into thymine, and only a smaller fraction is incorporated into the DNA.

An important factor to take into account was that those two studies also showed that the cell cycle has a crucial role in the DNA synthesis and the tritiated thymidine

incorporation into the DNA (16,60). Indeed, it seems that the precursor pool activity varies with the cell cycle, and that there is a significant increase in the S-phase and a small decrease in the G2-phase. Those observation, combined with the fact that the G1 cells are unable to take up thymidine, show that only cells in the S-phase can incorporate tritiated thymidine into the DNA. As mentioned above, our study focused on the *in vivo* exposure of zebrafish embryos and larva to tritiated thymidine, while most studies used to understand the underlying incorporation mechanisms were *in vitro* studies, most of them using synchronous cell suspensions. Differences in mechanisms could be discovered, as our study focuses on zebrafish embryos and larvae, organisms that undergo multiple cellular divisions, and that have a high renewal cell rate (29) More experiments would thus be needed in order to confirm the mechanisms associated with the tritiated thymidine incorporation in the whole fish and its DNA.

4.5. Microdosimetry

The simulations highlighted that low energy deposits had the highest probability, and that this probability decreased when the energy deposit increased. The spectrum also showed that the cells with the smallest radii have a higher probability of being a target for low energy deposits. Indeed, the maximum probability, only observed for the lowest energy deposit values, decreased when the cell radius increased (e.g. the probability of observing a small energy deposit for a spherical cell with a 0.25 µm radius was around 3 times higher than the one measured for a spherical cell with a 1.25 µm radius). After comparison of our spectrum with the one representing the kinetic energy of tritium (Supplementary Information, Figure S1), it seemed that, as highlighted by Morstin et al. in a microdosimetry study focusing on tritium, the low energy deposits were caused by low-energy electrons (24). Other microdosimetry studies also showed that for a same volume, the number of

deposition events decreased when the energy increased (61–63), which explains the results obtained in this study. In the smallest volumes (i.e. the cells with the lowest radius), only the low-energy electrons deposited their energy, because their deposit events were closer to each other. For electrons with a higher energy, the deposit events were farer from each other, meaning the risk of leaving the cell before depositing a significant amount of energy increased.

Those studies also explained another fact observed in our studies. After a small decrease of the probability when the imparted energy increased, an increase was observed, with the probability reaching a maximum at around 250 and 350 $eV.Bq^{-1}$ (for spherical and ellipsoidal cells, respectively). This increase was only visible for smaller cells (0.25-0.5 and 0.5 µm for spherical and ellipsoidal cells, respectively). After comparison of those spectrum with simulations made on cells with "no neighbours" (i.e. the electrons were only released in the cell of interest; Supplementary Information, Figure S2), it seemed that this increase was due to the presence of electrons in the neighbour cells. The microdosimetry studies presented above highlighted the fact that for a same volume, the number of deposition events decreased when the electron energy increased (24,61–63). This shows that the increase mentioned above should be caused by electrons with a slightly higher energy than the electrons causing the maximum probability.

Considering those two information, the increase reaching a maximum at around 250 and 350 $eV.Bq^{-1}$ should be caused by electrons with a slightly higher energy. Indeed, electrons with a higher energy travel longer paths between two interactions (i.e. energy deposits), causing a high proportion of the deposits to be out of the cell of interest. But when the electron starts its path in a neighbour cells, the chances that it ends its path, and thus deposits more energy, in the cell of interest, increases with increasing kinetic energy, thus increasing the probability of an energy deposit as shown in the spectrum. But as

explained above, this increase was only visible for small cells. This is due to the fact that high-energy electrons could also deposit more energy in larger cells, considering that the cell radius was sometimes bigger than the distance that electrons released by tritium during its decay can travel (i.e. 6 µm) (55). Thus, the deposits caused by electrons released in the neighbour cells that ended their path in the cell of interest represent a smaller proportion of the total energy deposit measured in the cell, which explains that the increase was not visible on the final spectrum.

The simulations also highlighted the fact that there was a non-linear relationship between the specific energy calculated in the cell and its radius. This is very interesting as it means that the specific energy can be calculated using the formula presented in Eq (3) and (4) for cells with radii ranging from 0.25 to 10 µm and from 0.5 to 15 µm (for spherical and ellipsoidal cells, respectively). Finally, the relationship between the specific energy and the cell radius showed that for an equal radius, the specific energy was lower in a spherical cell compared to an ellipsoidal one. This was expected, considering that the higher the mass of the target, the lower the specific energy will be. In the case of the cells studied here, for a same radius r, the volume of our ellipsoid is smaller than the volume of our sphere ($\frac{1}{3}\pi r^3$ vs $\frac{4}{3}\pi r^3$, respectively), which means that its mass is also smaller than the mass of the sphere.

Considering the fact that smaller cells present a higher probability of being the target of energy depositions closer to each other, it seems that those cells would be at a greater radiological risk than others. Indeed, several studies showed that low-energy electrons and more specifically tritium caused deleterious effects in zebrafish and other aquatic species (8,64–67). Considering the dimensions of the different cell types in the early-life stages of the zebrafish, the hypothesis is that smaller cells as dermal cells, chondrocytes or eye cells would be at a greater risk than notochord or mesodermal cells (i.e. 0.5 to 2 and 10 to 20

µm radii, respectively), considering that the energy deposits would be closer to each other (42,44,48,49,68).

5. Conclusion

This study successfully gave supplementary information on tritiated thymidine internalization in living organisms. We confirmed that after exposure of zebrafish early life stages to different tritiated thymidine activity concentrations, significant tritium levels could be measured in the whole fish and its DNA. We also confirmed that as for HTO, the internalization process is rapid, with the maximum activity concentration being measured in the sample after 24 hours of exposure. We also proved that tritium is completely internalized in its organic form, but that the chorion acts as a barrier to prevent the entrance of tritiated thymidine in the embryos. Though, significant levels could still be measured in the embryos once the chorion was removed. We also showed that the internal dose rate calculated for the embryos and larvae increased following a sigmoidal trend when the external activity concentration increased. This showed that there does not seem to be a gap between *in vivo* and *in vitro* studies when it comes to the tritiated thymidine internalization in the cells. Microdosimetric studies confirmed that the energy deposition probability and the mean energy deposited depend on the size of the cell considered, as well as its shape. It was shown that the energy imparted to the smallest cells came from the electrons with the lowest energy, thus increasing the risk of observing damages in those cells. It was also possible to find a linear fit between the mean imparted energy in the cell and the logarithm of its radius, highlighting that the quantity of energy deposited is proportional to the volume of the cell.

This study, being a part of a larger project, helped setting the perspective of using three of the activity concentrations studied and presented in this paper ($7.5x10^3$; $4x10^4$ and $1.1x10^5$ Bq/mL) in order to study the toxic effects of tritiated thymidine on zebrafish in its early life stages. Those activity concentrations were chosen as they lead to internal dose rates already used to study HTO and chronic gamma irradiation toxicity (22, 170 and 466µGy/h).

6. Acknowledgements

The authors would like to acknowledge IRSN for funding this project, as well as IRSN colleagues for their help on the experiments (Olivier Armant, Pierre Techer and Noëmie Guirandy), animal care (Elsa Cantabella) and liquid scintillation measurements (Daniel Orjollet).

References

1. IRSN. Tritium et environnement. 2014.
2. ASN. Livre Blanc du Tritium. 2010.
3. Arcanjo C, Maro D, Camilleri V, Cavalié I, Simon O, Beaugelin-Seiller K, et al. Assessing tritium internalisation in zebrafish early life stages: Importance of rapid isotopic exchange. J Environ Radioact. 2019;203:30–8.
4. Chen J. Radiation quality of tritium. Radiat Prot Dosimetry. 2006;122(1–4):546–8.
5. Jaeschke BC, Bradshaw C. Bioaccumulation of tritiated water in phytoplankton and trophic transfer of organically bound tritium to the blue mussel, *Mytilus edulis*. J Environ Radioact. 2013;115:28–33.
6. ASN. Livre blanc du Tritium & bilan des rejets de tritium pour les INB. 2018.
7. IRSN. Actualisation des connaissances acquises sur le tritium dans l'environnement. 2017.
8. Jaeschke BC, Millward GE, Moody AJ, Jha AN. Tissue-specific incorporation and genotoxicity of different forms of tritium in the marine mussel, *Mytilus edulis*. Environ Pollut. 2011;159(1):274–80.

9. McCubbin D, Leonard KS, Bailey TA, Williams J, Tossell P. Incorporation of Organic Tritium (3H) by Marine Organisms and Sediment in the Severn Estuary/Bristol Channel (UK). Mar Pollut Bull. 2001;42(10):852–63.

10. Gagnaire B, Adam-Guillermin C, Festarini A, Cavalié I, Della-Vedova C, Shultz C, et al. Effects of in situ exposure to tritiated natural environments: A multi-biomarker approach using the fathead minnow, *Pimephales promelas*. Sci Total Environ. 2017;599–600:597–611.

11. Gagnaire B, Gosselin I, Festarini A, Walsh S, Cavalié I, Adam-Guillermin C, et al. Effects of in vivo exposure to tritium: a multi-biomarker approach using the fathead minnow, *Pimephales promelas*. Environ Sci Pollut Res. 2020;27(4):3612–23.

12. Kim SB, Shultz C, Stuart M, Festarini A. Tritium uptake in rainbow trout (Oncorhynchus mykiss): HTO and OBT-spiked feed exposures simultaneously. Appl Radiat Isot. 2015;98:96–102.

13. Duque A, Rakic P. Different Effects of Bromodeoxyuridine and [3H]Thymidine Incorporation into DNA on Cell Proliferation, Position, and Fate. J Neurosci. 2011;31(42):15205–17.

14. Gray JW, Pallavicini MG, George YS, Groppi V, Look M, Dean PN. Rates of incorporation of radioactive molecules during the cell cycle. J Cell Physiol. 1981;108(2):135–44.

15. Hopwood LE, Dewey WC, Hejny W. Transport of thymidine during the cell cycle in mitotically synchronized CHO cells. Exp Cell Res. 1975;96(2):425–9.

16. Naito K, Skog S, Tribukait B, Andersson L, Hisazumi H. Cell cycle related [3H]thymidine uptake and its significance for the incorporation into DNA. Cell Prolif. 1987;20(4):447–57.

17. Peterson WJ, Tachiki KH, Yamaguchi DT. Extracellular matrix alters the relationship between tritiated thymidine incorporation and proliferation of MC3T3-E1 cells during osteogenesis in vitro. Cell Prolif. 2002;35(1):9–22.

18. Plagemann PGW, Richey DP, Zylka JM, Erbe J. Thymidine transport by Novikoff rat hepatoma cells synchronized by double hydroxyurea treatment. Exp Cell Res. 1974;83(2):303–10.

19. Zajicek G, Bernstein N, Rosin A, Gross J. Studies on the in vitro incorporation of tritiated thymidine into ascites tumor cells. Exp Cell Res. 1963;31(2):390–6.

20. Tang N, Bueno M, Meylan S, Incerti S, Tran HN, Vaurijoux A, et al. Influence of chromatin compaction on simulated early radiation-induced DNA damage using Geant4-DNA. Med Phys. 2019;46(3):1501–11.

21. Cruz GAS. Microdosimetry: Principles and applications. Rep Pract Oncol Radiother. 2016;21(2):135–9.

22. Kellerer AM, Chmelevsky D. Concepts of microdosimetry II. Probability distributions of the microdosimetric variables. Radiat Environ Biophys. 1975;12(3):205–16.

23. Chao T-C, Wang C-C, Li J, Li C, Tung C-J. Cellular- and micro-dosimetry of heterogeneously distributed tritium. Int J Radiat Biol. 2012;88(1–2):151–7.

24. Morstin K, Kopec M, Olko P, Schmitz T, Feinendegen LE. Microdosimetry of Tritium. Health Phys. 1993;65(6):648–56.

25. Ünak T, Selvi S. Microdosimetry of tritium and carbon-14 in different materials. Appl Radiat Isot. 1995;46(6):559–60.

26. Spence R, Gerlach G, Lawrence C, Smith C. The behaviour and ecology of the zebrafish, *Danio rerio*. Biol Rev. 2008;83(1):13–34.

27. Scholz S, Fischer S, Gündel U, Küster E, Luckenbach T, Voelker D. The zebrafish embryo model in environmental risk assessment—applications beyond acute toxicity testing. Environ Sci Pollut Res. 2008;15(5):394–404.

28. Fraysse B, Mons R, Garric J. Development of a zebrafish 4-day embryo-larval bioassay to assess toxicity of chemicals. Ecotoxicol Environ Saf. 2006;63(2):253–67.

29. Kimmel CB, Ballard WW, Kimmel SR, Ullmann B, Schilling TF. Stages of embryonic development of the zebrafish. Dev Dyn. 1995;203(3):253–310.

30. Westerfield M. The zebrafish book : A guide for the laboratory use of zebrafish *Danio (Brachydanio) rerio*. Institute of Neuroscience, University of Oregon; 1993.

31. Beaugelin-Seiller K, Jasserand F, Garnier-Laplace J, Gariel JC. Modeling radiological dose in non-human species: principles, computerization, and application. Health Phys. 2006;90(5):485–93.

32. Agostinelli S, Allison J, Amako K, Apostolakis J, Araujo H, Arce P, et al. Geant4—a simulation toolkit. Nucl Instrum Methods Phys Res Sect Accel Spectrometers Detect Assoc Equip. 2003;506(3):250–303.

33. Allison J, Amako K, Apostolakis J, Arce P, Asai M, Aso T, et al. Recent developments in Geant4. Nucl Instrum Methods Phys Res Sect Accel Spectrometers Detect Assoc Equip. 2016;835:186–225.

34. Incerti S, Baldacchino G, Bernal M, Capra R, Champion C, Francis Z, et al. The geant4-dna project. Int J Model Simul Sci Comput. 2010;01(02):157–78.

35. Incerti S, Ivanchenko A, Karamitros M, Mantero A, Moretto P, Tran HN, et al. Comparison of GEANT4 very low energy cross section models with experimental data in water. Med Phys. 2010;37(9):4692–708.

36. Bernal MA, Bordage MC, Brown JMC, Davídková M, Delage E, El Bitar Z, et al. Track structure modeling in liquid water: A review of the Geant4-DNA very low energy extension of the Geant4 Monte Carlo simulation toolkit. Phys Med. 2015;31(8):861–74.

37. Incerti S, Kyriakou I, Bernal MA, Bordage MC, Francis Z, Guatelli S, et al. Geant4-DNA example applications for track structure simulations in liquid water: A report from the Geant4-DNA Project. Med Phys. 2018;45(8):e722–39.

38. Salim R, Taherparvar P. Dosimetry assessment of theranostic Auger-emitting radionuclides in a micron-sized multicellular cluster model: A Monte Carlo study using Geant4-DNA simulations. Appl Radiat Isot. 2022;188:110380.

39. Braat AK, Zandbergen T, Water SVD, Goos HJT, Zivkovic D. Characterization of zebrafish primordial germ cells: Morphology and early distribution of vasa RNA. Dev Dyn. 1999;216(2):153–67.

40. Ciruna B, Jenny A, Lee D, Mlodzik M, Schier AF. Planar cell polarity signalling couples cell division and morphogenesis during neurulation. Nature. 2006;439(7073):220–4.

41. Concha ML, Adams RJ. Oriented cell divisions and cellular morphogenesis in the zebrafish gastrula and neurula: a time-lapse analysis. Development. 1998;125(6):983–94.

42. Easter Jr Stephen S, Nicola GN. The Development of Vision in the Zebrafish (*Danio rerio*). Dev Biol. 1996;180(2):646–63.

43. Field HA, Dong PDS, Beis D, Stainier DYR. Formation of the digestive system in zebrafish. ii. pancreas morphogenesis☆. Dev Biol. 2003;261(1):197–208.

44. Glickman NS, Kimmel CB, Jones MA, Adams RJ. Shaping the zebrafish notochord. Development. 2003;130(5):873–87.

45. Grandel H, Schulte-Merker S. The development of the paired fins in the Zebrafish (*Danio rerio*). Mech Dev. 1998;79(1):99–120.

46. Kane DA, Hammerschmidt M, Mullins MC, Maischein HM, Brand M, van Eeden FJ, et al. The zebrafish epiboly mutants. Development. 1996;123(1):47–55.

47. Kimmel CB, Miller CT, Moens CB. Specification and Morphogenesis of the Zebrafish Larval Head Skeleton. Dev Biol. 2001;233(2):239–57.

48. Li Q, Frank M, Thisse CI, Thisse BV, Uitto J. Zebrafish: A Model System to Study Heritable Skin Diseases. J Invest Dermatol. 2011;131(3):565–71.

49. Liu S, Narumi R, Ikeda N, Morita O, Tasaki J. Chemical-induced craniofacial anomalies caused by disruption of neural crest cell development in a zebrafish model. Dev Dyn. 2020;249(7):794–815.

50. Mizoguchi T, Verkade H, Heath JK, Kuroiwa A, Kikuchi Y. Sdf1/Cxcr4 signaling controls the dorsal migration of endodermal cells during zebrafish gastrulation. Development. 2008;135(15):2521–9.

51. Murakami T, Hijikata T, Matsukawa M, Ishikawa H, Yorifuji H. Zebrafish protocadherin 10 is involved in paraxial mesoderm development and somitogenesis. Dev Dyn. 2006;235(2):506–14.

52. Schmitt EA, Dowling JE. Early-eye morphogenesis in the zebrafish, *Brachydanio rerio*. J Comp Neurol. 1994;344(4):532–42.

53. Shin J, Park H-C, Topczewska JM, Mawdsley DJ, Appel B. Neural cell fate analysis in zebrafish using olig2 BAC transgenics. Methods Cell Sci. 2003;25(1):7–14.

54. Yin C, Solnica-Krezel L. Convergence and extension movements mediate the specification and fate maintenance of zebrafish slow muscle precursors. Dev Biol. 2007;304(1):141–55.

55. Carsten AL. Tritium in the Environment. In: Lett JT, Adler H, editors. Advances in Radiation Biology. Elsevier; 1979. p. 419–58.

56. Bonsignorio D, Perego L, Giacco LD, Cotelli F. Structure and macromolecular composition of the zebrafish egg chorion. Zygote. 1996;4(2):101–8.

57. Rawson DM, Zhang T, Kalicharan D, Jongebloed WL. Field emission scanning electron microscopy and transmission electron microscopy studies of the chorion, plasma membrane and syncytial layers of the gastrula-stage embryo of the zebrafish *Brachydanio rerio*: a consideration of the structural and functional relationships with respect to cryoprotectant penetration. Aquac Res. 2000;31(3):325–36.

58. van Pomeren M, Brun NR, Peijnenburg WJGM, Vijver MG. Exploring uptake and biodistribution of polystyrene (nano)particles in zebrafish embryos at different developmental stages. Aquat Toxicol. 2017;190:40–5.

59. Bourrachot S, Simon O, Gilbin R. The effects of waterborne uranium on the hatching success, development, and survival of early life stages of zebrafish (*Danio rerio*). Aquat Toxicol. 2008;90(1):29–36.

60. Cleaver JE, Holford RM. Investigations into the incorporation of [3H]thymidine into DNA in L-strain cells and the formation of a pool of phosphorylated derivatives during pulse labelling. Biochim Biophys Acta BBA - Nucleic Acids Protein Synth. 1965;103(4):654–71.

61. Turner JE, Paretzke HG, Hamm RN, Wright HA, Ritchie RH. Comparative Study of Electron Energy Deposition and Yields in Water in the Liquid and Vapor Phases. Radiat Res. 1982;92(1):47–60.

62. Liamsuwan T, Emfietzoglou D, Uehara S, Nikjoo H. Microdosimetry of low-energy electrons. Int J Radiat Biol. 2012;88(12):899–907.

63. Tung CJ, Chao TC, Hsieh HW, Chan WT. Low-energy electron interactions with liquid water and energy depositions in nanometric volumes. Nucl Instrum Methods Phys Res Sect B Beam Interact Mater At. 2007;262(2):231–9.

64. Arcanjo C, Adam-Guillermin C, Murat El Houdigui S, Loro G, Della-Vedova C, Cavalie I, et al. Effects of tritiated water on locomotion of zebrafish larvae: a new insight in tritium toxic effects on a vertebrate model species. Aquat Toxicol. 2020;219:105384.

65. Arcanjo C, Armant O, Floriani M, Cavalie I, Camilleri V, Simon O, et al. Tritiated water exposure disrupts myofibril structure and induces mis-regulation of eye opacity and DNA repair genes in zebrafish early life stages. Aquat Toxicol. 2018;200:114–26.

66. Beaton ED, Gosselin I, Festarini A, Gagnaire B, Farrow F, Cavalié I, et al. Correlated responses for DNA damage, phagocytosis activity and lysosomal function revealed in a comparison between field and laboratory studies: Fathead minnow exposed to tritium. Sci Total Environ. 2019;662:990–1002.

67. Adam-Guillermin C, Pereira S, Della-Vedova C, Hinton T, Garnier-Laplace J. Genotoxic and Reprotoxic Effects of Tritium and External Gamma Irradiation on Aquatic Animals. In: Whitacre DM, editor. Reviews of Environmental Contamination and Toxicology. Springer New York; 2012. p. 67–103.

68. Yin C, Kiskowski M, Pouille P-A, Farge E, Solnica-Krezel L. Cooperation of polarized cell intercalations drives convergence and extension of presomitic mesoderm during zebrafish gastrulation. J Cell Biol. 2008;180(1):221–32.

Tables

Table 1. Calculated dose coefficients for internal and external exposures (uGy/h per Bq/g) and fresh masses used in the dose rate calculations. Fresh masses have been measured and reported by Arcanjo et al. **(3)**.

Exposure duration (h)	**DCC_{ext} (µGy/h per Bq/g)**	**DCC_{int} (µGy/h per Bq/g)**	**Fresh mass (mg)**
24	$1.26x10^{-5}$	$2.24x10^{-3}$	1.18
96	$1.73x10^{-5}$	$2.24x10^{-3}$	0.25

Table 2. External activities (Bq/mL, n = 2-3 crystallizers) and dose rates (µGy/h, n = 10-15) measured in the water and the zebrafish embryos and larvae after 24 and 96 hours of exposure. Results are expressed as mean ± SD. - means that these data were not acquired during the corresponding experiment, or that the data could not be kept because of an issue in the experiment.

	After 24 hours of exposure		**After 96 hours of exposure**	
Starting activity (10^3 Bq/mL)	**External activity (10^3 Bq/mL)**	**Dose rate (µGy/h)**	**External activity (10^3 Bq/mL)**	**Dose rate (µGy/h)**
2.21	2.42 ± 0.38	15.50 ± 8.41	2.73 ± 0.56	6.03 ± 1.48
3.46	2.61 ± 0.30	17.38 ± 4.29	3.32 ± 0.08	15.19 ± 13.16
6.87	7.08 ± 1.29	22.09 ± 9.01	7.06 ± 0.36	22.75 ± 15.99
30.73	31.11 ± 0.20	121.58 ± 67.59	31.30 ± 1.96	65.36 ± 13.62
36.26	30.96 ± 0.23	120.48 ± 34.82	35.26 ± 0.31	76.80 ± 8.89
36.92	42.77 ± 4.97	234.78 ± 157.76	-	-
39.52	39.94 ± 0.06	263.34 ± 117.59	-	-
41.15	40.02± 1.15	252.06 ± 134.36	40.36 ± 4.99	98.88 ± 46.88
45.35	39.03 ± 3.73	282.21 ± 209.45	46.46 ± 2.70	83.36 ± 21.09
65.77	-	-	59.09 ± 3.41	103.76 ± 36.23
67.22	66.71 ± 1.19	267.36 ± 134.98	-	-
90.61	82.89 ± 1.65	615.71 ± 196.04	105.85 ± 10.58	70.14 ± 26.25
111.78	102.84 ± 3.00	785.28 ± 285.75	118.49 ± 5.68	146.24 ± 90.39
321.45	311.15 ± 8.15	907.86 ± 472.67	324.77 ± 10.16	663.98 ± 102.49
594.79	659.06 ± 28.91	1328.94 ± 485.48	627.40 ± 53.41	592.27 ± 60.42

804

805 **Table 3.** Total tritium and OBT dose rates (µGy/h, n=10-15) measured in the zebrafish embryos
806 after 24 hours of exposure. Results are expressed as mean ± SD. - means that these data were
807 not acquired during the corresponding experiment, or that the data could not be kept because of
808 an issue in the experiment. (t.test or Wilcoxon test, $p < 0.05$).

Starting activity concentration (Bq/mL)	Total tritium dose rate (µGy/h)	Total tritium dose rate (µGy/h)
$3.63x10^4$	120.48 ± 34.82	131.08 ± 49.82
$3.21x10^5$	907.86 ± 472.67	1046.63 ± 485.67
$5.95x10^5$	1328.94 ± 485.48	1462.89 ± 597.58

809

810

811 **Table 4.** Tritium activity concentration measured in the DNA (Bq/ug, n=3-5) extracted from
812 zebrafish embryos and larva after 24 and 96 hours of exposure, respectively. No significant
813 difference was found between 24 and 96 hpe for each activity concentration. (Kruskal-Wallis,
814 $a<b<c$, $A<B<C$, $p < 0.05$)

Starting activity concentration (Bq/mL)	Tritium activity concentration in the DNA after 24 hours of exposure (Bq/µg)	Tritium activity concentration in the DNA after 96 hours of exposure (Bq/µg)
$3.46x10^3$	0.25 ± 0.19^{a}	0.16 ± 0.05^{A}
$7.04x10^3$	0.31 ± 0.08^{ab}	0.25 ± 0.07^{AB}
$3.69x10^4$	1.22 ± 0.65^{b}	1.24 ± 0.49^{B}

815

816

817

Figures

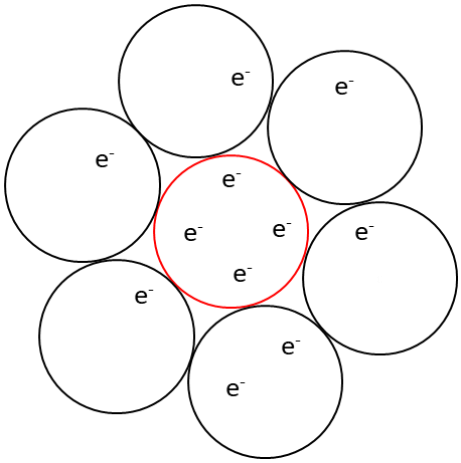

Figure 1. Schematic representation of the microdosimetry design used in the simulations. The red circle represents the cell of interest while the grey ones represent its neighbors. Electrons (e^-, 1E+06) were released in the cell of interest and its neighbors.

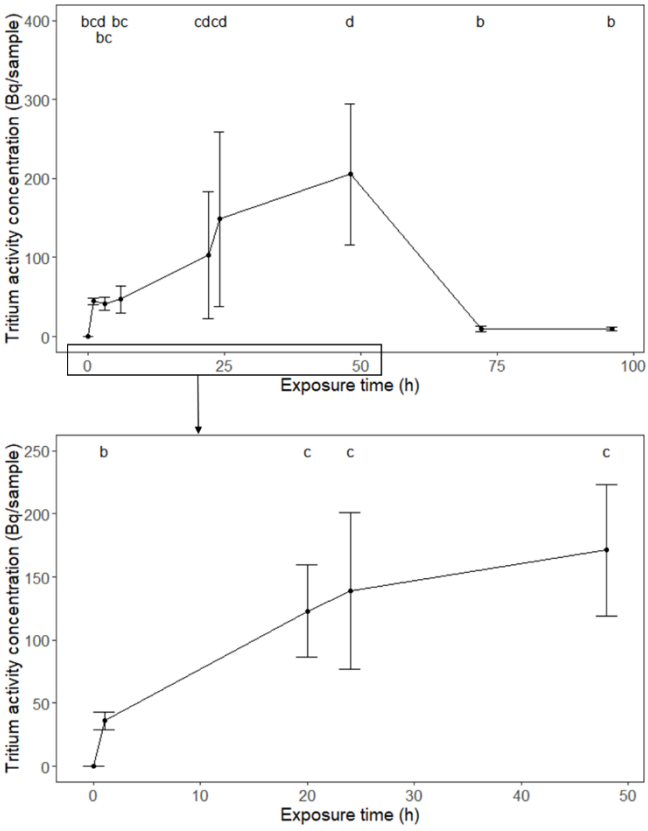

Figure 2. Tritium activity (Bq/sample, mean ± SD, n = 9-10) measured in individual samples after various exposure times to a tritium at an activity concentration of $4.5x10^4$ Bq/mL (top panel). The experiment repeated (bottom panel) on 15 individuals after a 1, 20, 24 and 48 h of exposure to a tritium at an activity concentration of $4x10^4$ Bq/mL (Kruskal-Wallis, a<b<c<d, $p < 0.05$, a corresponds to the basal tritium levels in the individual (< DL)).

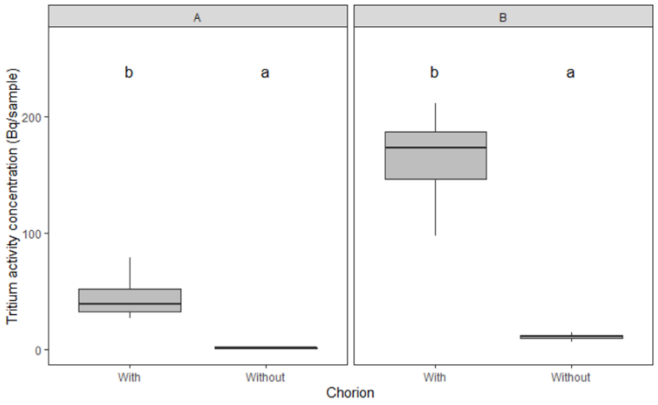

Figure 3. Tritium activity (Bq/sample, n = 15) measured in 51 hpf zebrafish embryo before and after the chorion removal. Those individuals were sampled after a 48 hour exposure to tritium at activity concentrations of $2.4x10^3$ (A, left panel) and $4.0x10^4$ (B, right panel) Bq/mL (statistical analysis: t.test, a<b, $p < 0.05$).

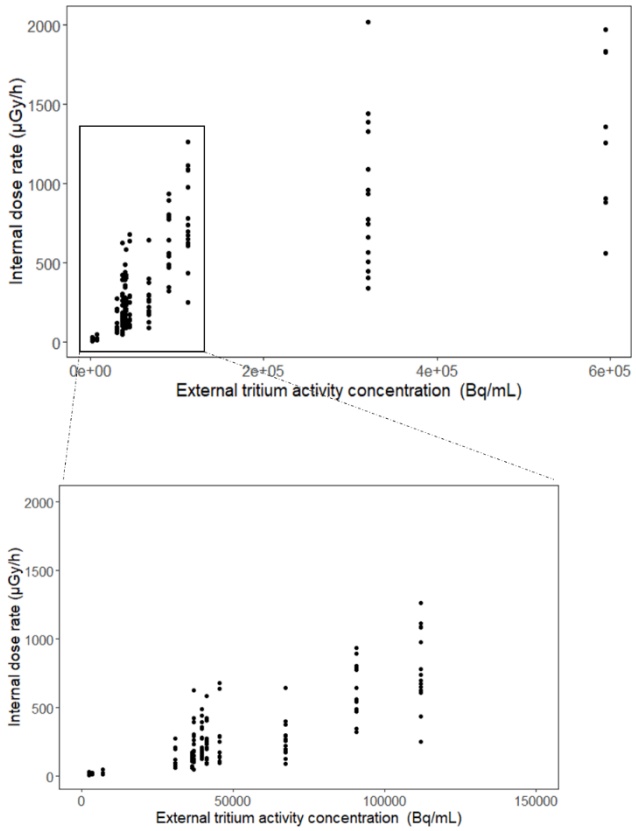

Figure 4. Variations in the internal dose rate (µGy/h, n=10-15) measured in zebrafish embryos after 24 hours of exposure to tritiated thymidine activity concentrations ranging from $2x10^3$ to $6x10^5$ Bq/mL. The graph was also zoomed around the 0 to $1.5x10^5$ Bq/mL region.

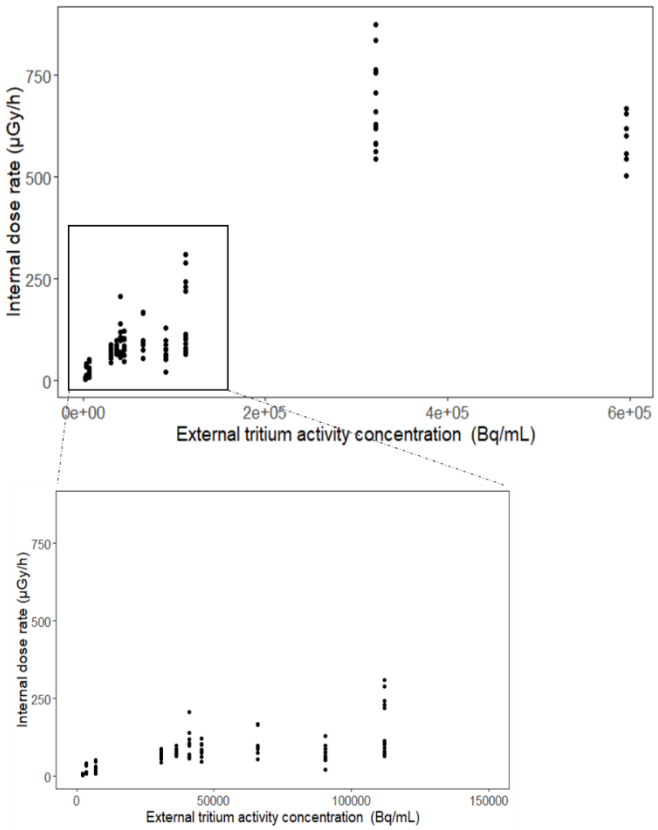

Figure 5. Variations in the internal dose rate (µGy/h, n=10-15) measured in zebrafish larvae after 96 hours of exposure to tritiated thymidine activity concentrations ranging from $2x10^3$ to $6x10^5$ Bq/mL. The graph was also zoomed around the 0 to $1.5x10^5$ Bq/mL region.

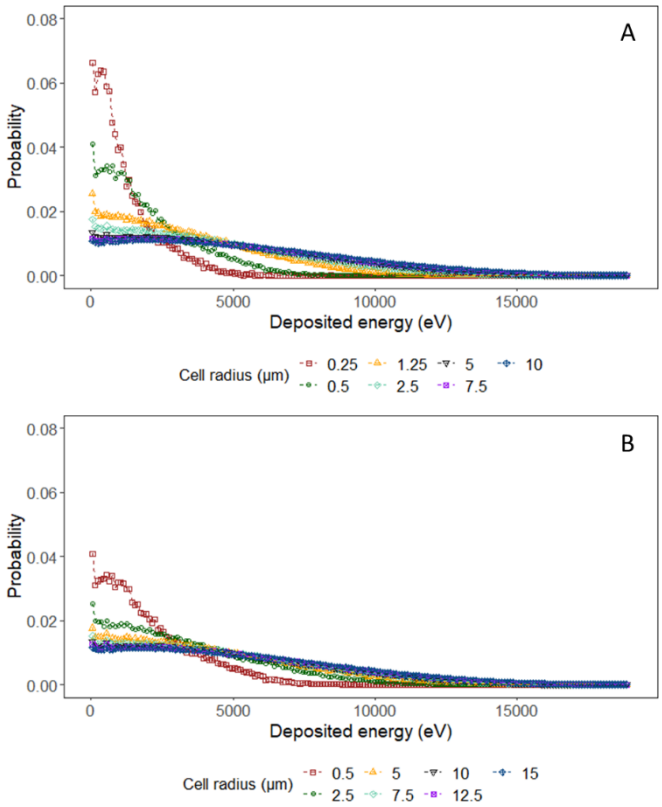

Figure 6. Energy deposited (eV, probability) in spherical (A) and ellipsoidal (B) cells of different radius (µm) by 1 Bq of tritium. Those results were obtained by the simulation of 10^6 electrons released in those same cells and their direct neighbours.

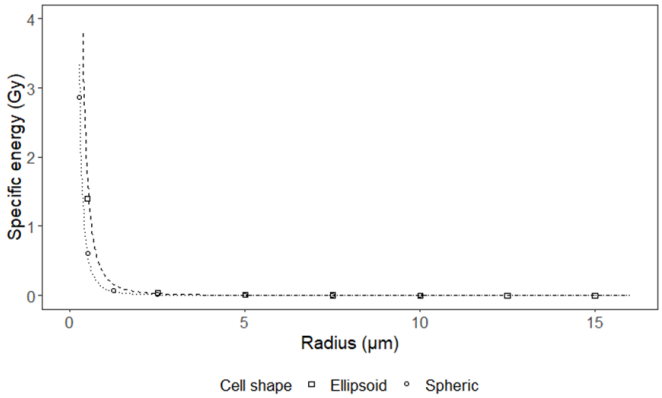

Figure 7. Specific energy (Gy) computed in spherical (circle) and ellipsoidal (square) cells of different radii (µm). The lines correspond to the equation representing the specific energy as a function of the radius of the spherical (dotted line) and ellipsoidal (dashed line) cells.

Supplementary Information

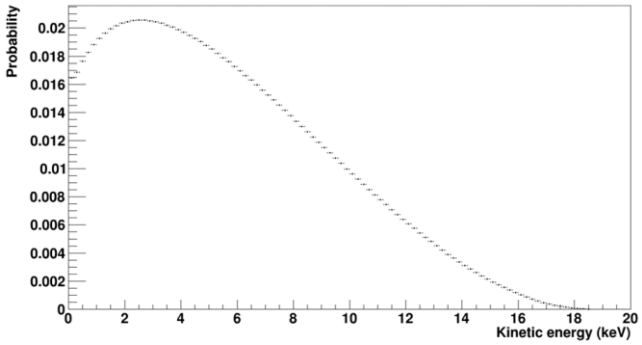

Figure S1. Tritium kinetic energy spectrum, representing the emission probability of an electron of a specific kinetic energy.

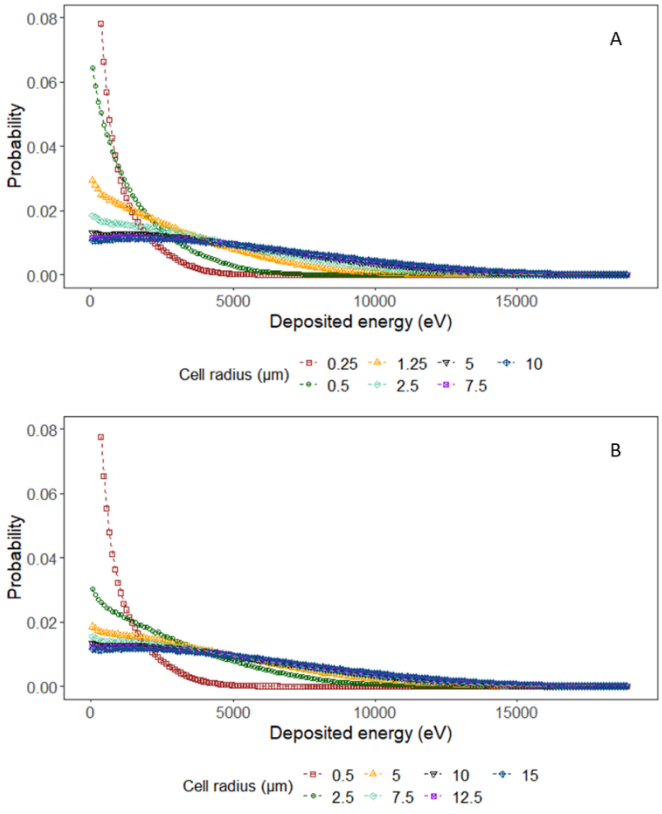

Figure S1. Energy deposited (eV, probability) in spherical (A) and ellipsoidal (B) cells of different radius (µm) by 1 Bq of tritium. Those results were obtained by the simulation of 10^6 electrons released in those same cells.